---

**Article:**
Hua, Y, Mohammed, S, Barker, R orcid.org/0000-0002-5106-6929 et al. (1 more author) (2020) Comparisons of corrosion behaviour for X65 and low Cr steels in high pressure CO2-saturated brine. Journal of Materials Science & Technology, 41. pp. 21-32. ISSN 1005-0302

https://doi.org/10.1016/j.jmst.2019.08.050

---

# Comparisons of corrosion behaviour for X65 and low Cr steels in high pressure $CO_2$-saturated brine

Yong Hua*, Sikiru Mohammed, Richard Barker and Anne Neville

Institute of Functional Surfaces, School of Mechanical Engineering, University of Leeds, Leeds, LS2 9JT, United Kingdom.

*Corresponding author: Yong Hua, Ph.D., Tel: +44 (0) 7923359918, fax: +44 (0) 1132424611.

*Email address:* menyh@leeds.ac.uk (Y. Hua)

Appropriate material selection for injection pipelines and tubing for carbon dioxide geologic storage is fundamental to ensure asset integrity and reduce cost. This paper evaluates the corrosion behaviour of X65, 1Cr, 3Cr and 5Cr, which have the potential to be utilised as injection pipeline/tubing materials. The influence of steel Cr content on the general and localised corrosion behaviour is investigated at time periods from 6 to 192 hours at 60°C and 100 bar. The evolution, morphology and chemistry of corrosion products on the surface of each material were evaluated using a combination of Scanning Electron Microscopy, Energy Dispersive X-Ray Spectroscopy and X-Ray Diffraction and related to their overall corrosion protection. Results indicate that prior to the formation of protective films on the steel surfaces, the resistance of the materials to corrosion increase with increasing Cr content (Corrosion resistance: X65<1Cr<3Cr<5Cr). However, as corrosion products evolve, the protection afforded to the different steels varies significantly and decreases with increasing Cr content. X65 becomes the material with the lowest general corrosion rate by the end of the 192 h experiments and 5Cr exhibits the highest corrosion rate (ranking of corrosion resistance: X65>1Cr>3Cr>5Cr). In terms of the corrosion products on X65, both inner amorphous and outer crystalline corrosion layers consist of $FeCO_3$. For the Cr-containing steels, the outer layer also comprises $FeCO_3$, but the inner layer is enriched with Cr, and is predominantly amorphous $Cr(OH)_3$. The extent of localised corrosion (determined using surface profilometry) is noticeably less for X65 compared to the Cr-containing steels. The paper raises questions about the benefits that low Cr steels offer towards extending component design life compared to carbon steel under the test conditions considered here.

**Key words: carbon dioxide, corrosion, X65, low-Cr steels, iron carbonate, chromium hydroxide**

## *1. Introduction*

Carbon capture and storage is considered as one of the main technologies available to assist in the abatement of climate change. The process has the potential to enable significant sequestration of high pressure carbon dioxide ($CO_2$) in both depleted oil and gas fields and geological reservoirs. $CO_2$ injection can also be used for the purposes of enhanced oil recovery to extend the lifetime of oil and gas reservoirs.

Given the processes involved in $CO_2$ sequestration, corrosion of equipment can occur when large amounts of $CO_2$ in the dense phase are injected into storage sites. The injection pipeline receives compressed $CO_2$ typically in a liquid or supercritical state. When continuous injection is performed down a vertical line, water is displaced from the head of the pipeline. If the continuous process is ever interrupted, brine will proceed to flow back to the injection point, potentially rising hundreds of meters up the injection line before equilibrium is re-established[1]. Consequently, during this period the injection materials become exposed to a saline solution saturated with high pressure $CO_2$. These sections of the line which are in contact with the $CO_2$-containing brine can suffer particularly high levels of corrosion. Based on this, it is important to understand the corrosion severity under such static conditions and to select appropriate materials to ensure the integrity of the line for the duration of its intended operation.

The most cost-effective material for injection systems from the perspective of capital expenditure is carbon steel. However, this material is notoriously susceptible to $CO_2$ corrosion in the absence of protective corrosion products, making it prudent to also consider alternative materials to reduce operational expenditure if a particularly long design life is required [1, 2, 3]. Past research has highlighted the potential of low chromium (Cr) containing steels to offer improved strength, hardenability and corrosion resistance compared to carbon steel[4, 5, 6, 7]. These steels typically contain between 1 and 5% Cr and can provide a cost effective alternative compared to corrosion resistant alloys (CRAs)[5, 6, 7, 8, 9, 10, 11, 12, 13]. Kermani and Morshed[9] suggested that the use of 1-5Cr steel can improve the $CO_2$ corrosion resistance by a factor of 2.5-40 with a cost penalty less than 1.5 times that of carbon steel.

There is a wealth of research reaching back to the 1980's[1, 7, 8, 10, 14, 15, 16, 17, 18, 19] focusing on the influence of 1-5% Cr addition to steels to improve strength, hardenability and $CO_2$

corrosion resistance, with the majority of observations concluding that Cr addition does improve corrosion performance[7, 10]. In addition, a number of successful field trials have been reported[14, 20] with the use of low Cr alloyed steels. However, a handful of researchers have identified adverse effects of Cr addition (i.e, a reduction in corrosion resistance of low alloyed steel with increasing Cr content) [14, 21, 22, 23] under specific operating conditions, presenting conflicting observations. Amit et al.,[23] reported 3Cr steel has a higher corrosion rate of 0.78 mm/year compared to the corrosion rate of 0.23 mm/year for 1Cr steel at 135°C.

One critical observation is the role of Cr-containing steel on influencing the chemistry, structure and morphology of corrosion products and how they contrast with corrosion products on carbon steels. In the majority of experiments, researchers have reported that corrosion rates begin to decline as protective corrosion products establish themselves[24, 25]. In simple $CO_2$-containing brines with only sodium chloride (NaCl) as a dissolved salt, authors have reported the corrosion product iron carbonate ($FeCO_3$) developing on carbon steel which assists in mitigating corrosion. However, for Cr-containing low alloy steels, the films can become enriched with undissolved Cr and some of its compounds, supposedly facilitating better general and localised corrosion protection[1, 16, 26, 27]. Researchers have also reported the development of duplex structures of the corrosion film on Cr-containing steels, consisting of an inner and outer layer[21, 26]. The Cr-enrichment of the inner film was believed to not only provide superior general and localised corrosion protection, but also assist in the prevention of local destruction of films by mechanically strengthening the corrosion product[21, 26].

Despite an abundance of research into the potential advantages of low Cr alloyed steels, nearly all of the aforementioned studies have been conducted in environments at relatively low pressure where $CO_2$ exists in its gaseous state and conditions are more akin to what is seen in oil and gas transport, not in high pressure $CO_2$ injection. A few exceptions to this exist whereby Hassani et al.[15] evaluated the behaviour of 1018 carbon steel, 5Cr and 13Cr at 80 bar $CO_2$ and 60°C and indicated that 5Cr was 3 times more corrosion resistant than carbon steel under such conditions, yet still produced a corrosion rate of 6 mm/year over 42 h of immersion. Pfennig et al.[28] also determined the corrosion resistance of 1Cr and 13Cr in both the brine and supercritical $CO_2$ phase at 100 bar and 60°C. Their research suggested that 1Cr was capable of handling the $CO_2$ stream conditions and the $CO_2$-saturated brine phase, producing corrosion

rates comparable to 13Cr over 8000 h exposure, below 0.2 mm/year. However, no comparison was made with carbon steel, 3Cr or 5Cr under these specific conditions or across non-film forming conditions.

This paper addresses the knowledge gap in the area of low Cr alloy behaviour in static high pressure $CO_2$ environments by evaluating the corrosion response of four different steels (X65, 1Cr, 3Cr and 5Cr) over time periods between 6 and 192 h at 60°C and 100 bar in a 1 wt.% NaCl solution. By examining all four materials, the influence of Cr content within the steel on the general and localised corrosion behaviour is investigated. The evolution, morphology and chemistry of corrosion products on the surface of each material are evaluated over time periods of 6, 24, 48, 96 and 192 h and related to the level of localised and general corrosion protection. In these experiments, a high surface area to volume ratio was deliberately chosen to generate significant film formation in a shorter timeframe. To understand the film formation characteristics, a combination of short duration and long duration experiments was performed. The focus of the short term (6 h) experiments was predominantly to understand the corrosion behaviour of the steels in the absence of protective corrosion products. These experiments can be thought of as more analogous to field conditions in an environment with a solution under-saturated with respect to various corrosion products. In longer duration tests, it is appreciated that a new set of equilibrium conditions become established at higher pH and greater $Fe^{2+}$ concentration in the bulk solution, which is a limitation of the closed system test methodology. However, the focus from long term experiments (192 h) is to determine the nature of the films developed when precipitation does occur and to evaluate the extent of protection they offer to the substrate in relation to both general and localised corrosion.

The experiments conducted within this paper attempt to simulate the process encountered during intermittent injection of $CO_2$, whereby the brine rises back up the pipeline when injection ceases for a number of days. In this situation, a static fluid with a fixed volume is in contact with a specific internal area of pipeline.

## *2. Experimental Procedure*

### *2.1 Materials and Preparation*

All corrosion rates were measured based on gravimetric analysis of test specimens exposed to the brine solution for different durations between 6 and 192 h using a 1 L stainless steel autoclave. Mass loss specimens were machined from X65 carbon steel, 1Cr, 3Cr and 5Cr steel bars into discs of diameter 25 mm and thickness of 6 mm (an image of the prepared sample is embedded in Figure 1(a)). The chemical compositions of each of the materials considered are provided in Table 1. Surface preparation consisted of wet-grinding the entire sample surface with 600 grit silicon carbide (SiC) abrasive paper, rinsing with distilled water, followed by acetone, high purity ethanol and drying gently with compressed air. Samples were then stored in a desiccator until needed and weighed immediately before use on an electronic balance to within an accuracy of 0.01 mg before suspending inside the autoclave. Two samples were placed in the autoclave for each test, with experiments being repeated a minimum of 3 times.

### *2.2 Microstructural characterisation*

Surface preparation for microstructural characterisation consisted of wet-grinding one sample surface up to 1200 grit SiC abrasive paper, followed by polishing using a polishing cloth with a 3 µm diamond suspension to attain a mirror finish. Etchant concentration was varied depending on the sample alloy composition in accordance with in ASTM E3-01[29] and E407-99 standards[30]. 2-5 % Nital solution was used for the different materials, with etching time varying from 10-20 seconds. Microstructural analysis was carried out using a LEICA DM 6000M upright optical microscope.

The microstructures of X65, 1Cr, 3Cr and 5Cr samples are presented in Figure 1. A ferritic-pearlitic microstructure is observed for X65 carbon steel. The microstructure of 3Cr shows carbides randomly distributed and the microstructure of 5Cr indicated carbides as dark areas in a ferrite matrix, while 1Cr shows an inhomogeneous distribution of martensite and ferrite.

### *2.3 Mass loss tests*

A schematic representation of the autoclave experimental setup is provided in Figure 2 [31, 32, 33]. The 1 wt.% NaCl solution used in each experiment was de-aerated by saturating the solution with $CO_2$ in a separate container for a minimum of 12 h prior to testing. The specimens were suspended within the autoclave using a non-conducting wire whilst also ensuring they were not in contact with the walls of the cylinder to prevent galvanic effects. The prepared, $CO_2$-

147 saturated water was carefully delivered into the autoclave at ambient pressure and temperature
148 and sealed. All lines to the autoclave were then purged with $CO_2$ and evacuated to ensure
149 complete removal of oxygen within the system. The $CO_2$ was then transferred into the autoclave
150 and heated and pressurised to the required temperature and pressure. The starting point of
151 each test was taken from the time at which the autoclave reached the desired temperature and
152 pressure of 60°C and 100 bar, respectively. Experiments for each material were conducted for
153 6, 24, 48, 96 and 192 h to determine the changes in corrosion rate with time in static conditions.
154 MultiScale[34] software was used to calculate the initial pH of the brine solution and was
155 determined to be approximately 3.1 under the specified conditions.

156 Upon completion of each test, the specimens were dried thoroughly. They were then
157 weighed and chemically cleaned to remove all traces of corrosion products before weighing
158 again to determine the mass of corrosion product on the steel surface as well as the corrosion
159 rate. The cleaning process consisted of wiping the surface with a cotton pad soaked in Clarke's
160 solution (20 g antimony trioxide + 50 g stannous chloride + 1000 ml 38% hydrochloric acid) in
161 accordance with ASTM Standard G1-03[35]. After cleaning, samples were rinsed with distilled
162 water, followed by ethanol, before being dried with compressed air.

163 The mass loss due to corrosion was determined from the mass difference before exposure
164 and after cleaning. The corrosion product mass is the difference before and after chemical
165 cleaning, after exposure to the test environment.

166 The corrosion rates were calculated by using Equation (1):

$$V_c = \frac{87600\Delta m}{\rho A T} \quad (1)$$

167 Where $V_C$ is the corrosion rate of the sample in mm/y, $\Delta m$ is the mass loss in grams, $\rho$ is the
168 density of the sample in g/cm$^3$, $A$ is the exposed area in cm$^2$ and $T$ is the immersion time in hours.

169 ***2.4 Characterisation of corrosion products***

170 The surface coverage and morphology of the corrosion products were characterised using
171 a Carl Zeiss EVO MA15 SEM. Raman spectroscopy was used to identify the nature of the

corrosion products locally on the surface and to detect the presence of potentially amorphous products not recorded by XRD.

### *2.5 Interferometry*

Post-test profilometry measurements were performed on samples (scanning a 3 x 3 $mm^2$ area at a time) using a $NP_{FLEX}$ 3D Surface Metrology System to quantify localised attack. The objective used 10x magnification with approximately a 3.5 mm working distance. The pit depth analysis was conducted in alignment with ASTM Standard G46-94[36]. The standard stipulates that an average of the 10 deepest pits should be used for pit damage characterisation of the sample area.

## *3 Results*

### *3.1 The effect of steel Cr content on general corrosion rate in a $CO_2$-saturated solution at 60°C and 100 bar*

Figure 3 presents the total mass loss and general corrosion rates of X65, 1Cr, 3Cr and 5Cr steel exposed to $CO_2$-saturated 1 wt.% NaCl solution at 60°C and 100 bar for various immersion times from 6 and 192 h. Figure 3(a) expresses the mass loss as a function of time, while Figure 3(b) indicates the average corrosion rates in mm/year for each material from 6 h to 192 h, assuming a uniform thickness loss over the steel surface.

Referring to Figure 3(b), during the initial 6 h, the highest corrosion rate of 16.6 mm/year was observed for X65 carbon steel. The general corrosion rate over the first 6 h for each material decreased as Cr content increased; the general corrosion rate for 5Cr was 6.7 mm/year, which was 2.5 times lower than X65 carbon steel. SEM images later in this paper indicate iron carbide ($Fe_3C$) exposure due to the fast and selective dissolution of ferrite for X65. The images also indicate that the corrosion products on the carbon steel surface are minimal over this period. For the different Cr steels, a corrosion product layer was already evident on the steel surface after 6 h.

The general corrosion rates of X65, 1Cr, 3Cr and 5Cr steel over 192 h were 1.5, 1.9, 2.0 and 2.1 mm/year, respectively. Despite the materials showing a clear benefit of higher Cr content during the initial 6 h, longer duration tests reflect that Cr addition has much less benefit in terms

of material dissolution, arguably demonstrating a negative effect on long-term corrosion behaviour in the closed system. This difference in corrosion rate is actually more significant than the 192 h average corrosion rates indicate. For example, by considering the time intervals and mass loss between 96 and 192 h in Figure 3(a), X65, 1Cr, 3Cr and 5Cr have corrosion rates of ~0.01, 0.10, 0.75 and 1.32 mm/year which is much more significant than the integrated corrosion rates represented in Figure 3(b).

The reduction in corrosion rates over the duration of 192 h for all samples is likely attributed to the formation of protective corrosion products on the steel surface. The following sections of this paper focus on identifying the key differences between the film structures, morphology and composition in an effort to understand the difference between the four materials in terms of their corrosion rates.

### *3.2 The influence of immersion time on corrosion product morphology – X65 and 5Cr*

The largest difference in general corrosion rate was observed for X65 and 5Cr as expected. Consequently the evolution of corrosion products on these two surfaces was studied in detail using SEM. Images of the top surface morphology formed on X65 carbon steel and 5Cr at various immersion times are shown in Figure 4, and the corresponding cross-sections featuring the thickness of corrosion products are provided in Figures 4 and 5.

After the first 6 h, a thin $Fe_3C$ layer of approximately 1 µm appeared on the X65 steel surface due to the high rate of ferrite dissolution (Figure 4(a)). (Confirmation of the revealing of this $Fe_3C$ layer is provided using XRD in our previous publication.[31]) Crystals then began to cover the steel surface after 24 h (shown in Figure 4(b)). Although the layer developed after 24 h was 30 µm thick, gaps in the corrosion product were still visible where the electrolyte could easily access the steel substrate. After 96 h, a dense and more compact layer covered the entire surface and increased to a relatively uniform thickness of 60-65 µm. This layer contributed towards a reduction in corrosion rate. No significant change in the film morphology was observed beyond 96 h as shown in Figure 4(c) and 4(d).

To compare with the corrosion products formed on X65 carbon steel, Figure 4(e) – (h) presents the SEM top view images of 5Cr steel exposed to the $CO_2$-satuated solution at 60°C and 100 bar for various immersion times (with corresponding cross-sections in Figure 6). The SEM

images of the 5Cr steel surface showed a very different structure over the first 24 h of exposure compared to X65 steel. The images in Figures 4(e) and (f) feature a dehydrated/cracked, seemingly amorphous corrosion product film on the surface (based on cross-sections provided in Figures 6(a) to (c)). There was no difference in top view morphologies between 6 and 24 h, however, the thickness of the corrosion product layer increased from 1 µm to 10 µm (see Figures 6(a) and (b)). It is clear from these images that the corrosion product which develops on the low Cr steel is generated very quickly and this may be responsible for its superior corrosion resistance compared to X65 in the early stages of corrosion. However, it is important to stress that although this amorphous film may result in a lower corrosion rate/mass loss compared to X65 over the first 24 h in Figure 3(a), the corrosion rate of 5Cr is still ~4.5 mm/year between 6 and 24 h based on mass loss values.

Crystals became visible under the SEM after 96 h exposure of 5Cr to the test solution (Figure 4(g)), and were randomly distributed on top of the initially developed layer. After 192 h of exposure (Figure 4(h)) the corrosion product produced a two-layer structure and the formed crystals started to cover the entire surface. The thickness of the corrosion product layer measured approximately 60 µm after 192 h, which was very similar to that of X65 at the same exposure time. However, in contrast to the crystalline film observed on X65 steel after 192 h, there are still identifiable gaps between crystals. Comparing the development of the crystals in Figures 4(f), (g) and (h) with the mass loss values for 5Cr in Figure 3(a), the rate of mass loss does not change significantly from 24 to 192 h. A relatively linear increase in mass loss is observed with time, despite the crystals clearly developing on the steel surface. This suggests that the inner amorphous layer is dictating the corrosion response of the steel surface, which is sensible given the crystals are not in direct contact with the substrate and appear not to present a particularly resistant diffusion barrier based on SEM analysis. Such behaviour contrasts with that of X65 steel under the same conditions where a more compact crystalline film has developed over the same time period.

### *3.3 Characterisation of two-layered corrosion product*

To understand the chemistry of the two-layered corrosion product, a combination of energy dispersive x-ray (EDX), XRD and Raman spectroscopy was employed. The EDX analysis of X65, 1Cr, 3Cr and 5Cr steel cross-sections and element distribution maps of the corrosion

product layers after 192 h of immersion are presented in Figure 7. The results show that the thickness of the corrosion products for X65, 1Cr, 3Cr and 5Cr are similar, reaching approximately 60 µm after 192 h exposure. Additionally, all samples display a duplex, or double layered structure comprising of an inner and outer layer. For X65 steel, the inner and outer layer chemical composition is very similar, comprising of mainly Fe, C and O. However, in the case of the Cr-containing steels, the inner layer contained significant levels of Cr, exhibiting a greater intensity in the EDX maps than that of the steel microstructure. This enrichment of Cr was particularly high at the interface between the inner and outer layer. Referring to Figure 3 and Figure 6, it is the formation of this inner Cr-rich layer on the low Cr-containing steels which contributes most towards the corrosion resistance and reduces the corrosion rates. In terms of the outer layers on the Cr-steels, only Fe, C, and O could be identified, with minimal Cr being detected.

To identify the nature of the corrosion product layers on different steel surfaces after 192 h, XRD measurements were also conducted. The corresponding patterns provided in Figure 8 showed that the only crystalline phase detected on all materials after 192 h was $FeCO_3$ which relates to the crystals clearly visible on the outer layer. This observation agrees with the work done by Nazari et al.,[37] who indicated that $FeCO_3$ formed on X70 samples exposed to 65°C and pH in the range of 5.5-6.5. No traces of crystalline Cr compounds within the corrosion product layer were detected on any of Cr-containing steels using XRD, indicating that the products are nano-crystalline or amorphous. This observation corroborates with the work of Guo et al.,[10] who showed through Transmission Electron Microscopy (TEM) analysis, that the inner layer of 2Cr exposed to a $CO_2$-containing environment possessed an amorphous structure. Raman spectroscopy was used to further identify the inner film on both X65 and the low Cr steels. The spectra provided in Figure 9 relate to two scans conducted on 5Cr steel; one on the outer layer, and one on the inner layer which was analysed through the gaps present in the outer layer. The spectra are representative of the scans obtained on all three Cr-steels in that for the outer layer, three peaks located at 290, 743 and 1086 $cm^{-1}$ confirmed the presence of $FeCO_3$ (blue spectra – Region A) and one peak located at 713 $cm^{-1}$ for the scan on the inner layer confirmed the presence of chromium hydroxide ($Cr(OH)_3$) (red spectra – Region B). In some spectra, traces of $FeCO_3$ (potentially amorphous or nano-crystalline) were also detected within the inner layer, though this mainly comprised of $Cr(OH)_3$. Similar observations of $Cr(OH)_3$ have been reported

by Xu et al.,[6] who evaluated the corrosion behaviour of 1-6.5Cr steels in $CO_2$-saturated formation water. They also reported that the inner amorphous layer is mainly comprised of $Cr(OH)_3$ by Raman analysis, with the detected main $Cr(OH)_3$ peak being observed at 713 $cm^{-1}$ by scanning $Cr(OH)_3$ powders. Similar conclusions were also made by Guo et al.,[10] who used TEM and XPS analysis to identify the inner layer of 2Cr steel and observed it is comprised of amorphous $FeCO_3$ and $Cr(OH)_3$. Xu et al.[5] also studied the corrosion behaviour of 3Cr steel in $CO_2$-satuated formation water at 80°C and 8 bar $pCO_2$ and have reported the same double layer structure consisting of a crystalline $FeCO_3$ layer on the top of an inner amorphous Cr-rich layer.

### *3.4 Corrosion product mass and localised corrosion behaviour*

In addition to evaluating the role of corrosion product growth on the general corrosion behaviour, consideration is also afforded here to the propagation of pits on each steel surface as a function of time.

Surface profilometry measurements (examples provided in Figure 10) were performed after corrosion products were removed using Clarke's solution on every material after exposure to the test solution for 6, 24, 48, 96 and 192 h. Figure 11 shows the mass of the corrosion products formed on sample surfaces and the localised depth for X65, 1Cr, 3Cr and 5Cr steel exposed to $CO_2$-saurated solution at 60°C and 100 bar for various immersion times.

For X65, the compact $FeCO_3$ layer provides protection against localised corrosion beyond 96 h. However, 1Cr, 3Cr and 5Cr steels show higher localised attack which continues to propagate over the entire 192 h period. The localised depth of 1Cr, 3Cr and 5Cr exceeded that of X65, with 1Cr being the most susceptible to localised corrosion with a pit depth of 62 µm after 192 h. Interestingly, the $FeCO_3$ inner layer on X65 steel suppresses pit propagation, while the inner layer which develops on 1Cr, 3Cr and 5Cr (which mainly comprises of $Cr(OH)_3$) fails to fully suppress pit propagation over 192 h.

### **3.5 Solution replenishment experiments to confirm film protective properties**

This research highlights that prior to the formation of a fully protective $FeCO_3$ layer on the steel surface, the corrosion resistance of the materials increased with increasing Cr content, agreeing with previous studies[7, 10]. However, an important message from this work is that as

the corrosion products grow over 192 h, the protection afforded to the different steels decreases with increasing Cr content. The results in Figure 3 show that X65 has the lowest corrosion rate after 192 hours exposure and 5Cr becomes the material with highest corrosion rate. The results also highlight the limitations of inferring corrosion behaviour of materials and their ranking based on experiments over individual fixed time intervals. For example, referring back to Figure 3, any single set of mass loss measurements at a particular time interval before 96 h would produce the conclusion that increasing Cr content in the steel improves general corrosion resistance. However, extended tests performed in this work show this is not the case for this particular environment beyond 96 h if a corrosion product is capable of developing on the steel surface.

As discussed earlier in this paper, a limitation of the closed vessel experiment is the change in brine chemistry as a function of time and the consequences this has on the corrosion products formation as well as material corrosion behaviour. In order to address this issue and ensure the correct conclusions are made regarding the protectiveness of the corrosion products developed, solution replenishing was conducted after 48 h for X65 and 5Cr steel. At this instance in time, a fully formed $FeCO_3$ layer was present on X65 steel (shown by the stable corrosion product mass in Figure 11(a)), while solely the amorphous $Cr(OH)_3$ layer was established on the 5Cr steel. The effect of solution replenishing is shown in Figure 12, which represents the average corrosion rate over 192 h. The results show that the films formed on X65 and 5Cr after 48 h are as protective as the 192 h data in Figure 3(b) suggests. This is important as the reduction in corrosion rate with time could be attributed to the change in solution chemistry, not the establishment of the film, and it is important to decouple these effects from one another to understand the true protectiveness of the developed corrosion products.

## *4.0 Discussions*

### *4.1* Development of the duplex corrosion product

The corrosion of carbon steel and low Cr steels in $CO_2$-containing brines is facilitated through the hydration of $CO_2$ which produces carbonic acid ($H_2CO_3$). The dissociation of $H_2CO_3$ in two steps produces the acidity ($H^+$) within the aqueous phase.

346 The cathodic reactions of steel are related to the reduction of $H^+$ ions which are either
347 supplied directly, or provided through the dissociation of $H_2CO_3$ at the steel surface via a
348 buffering effect[38]. The resulting anodic reactions are either the dissolution of iron, chromium,
349 or both into the solution, depending on the material composition:

$$Fe_{(s)} \rightarrow Fe^{2+}_{(aq)} + 2e^- \quad (2)$$

$$Cr_{(s)} \rightarrow Cr^{3+}_{(aq)} + 3e^- \quad (3)$$

350 The formation of the corrosion products such as $FeCO_3$ and $Cr(OH)_3$ has been reported by
351 several researchers in $CO_2$ environments[10, 39, 40] and occur when the products exceed their
352 solubility locally within the system, resulting in precipitation onto the surface of the steel,
353 typically via the following proposed processes:

$$Fe^{2+}_{(aq)} + CO^{2-}_{3(aq)} \rightarrow FeCO_{3(s)} \quad (4)$$

$$Cr^{3+} + 3OH^- \rightarrow Cr(OH)_3 \quad (5)$$

354 Based on the corrosion product analysis described previously, a schematic representation
355 of the corrosion product formation processes on the four steel surfaces is provided in Figure 13.
356 With respect to X65 steel, the inner and outer layers begin to form at very similar times[31], with
357 the inner layer displaying less signs of crystallinity. However, from the perspective of the Cr
358 steels, the inner amorphous layer (which is predominantly $Cr(OH)_3$, with potential traces of
359 amorphous/nano-crystalline $FeCO_3$) clearly develops first. Once this layer reaches a critical level
360 of protectiveness/thickness, it is followed by the precipitation of the outer crystalline $FeCO_3$
361 layer. Given the significant reduction in corrosion rate with time in the early stages of the Cr
362 steels exposure, the majority, if not all of the protection is facilitated by the inner layer.

363 Furthermore, the Cr enrichment within the inner layer increases with the Cr content of the
364 steel and this Cr-rich layer provides the corrosion protection, however, the protective nature of
365 these layers in the context of general corrosion reduces with increasing steel Cr content.

366 The effect of Cr enrichment also appears to have implications for localised corrosion, with
367 a higher pit depth being recorded after 192 h for the Cr steels compared to X65. The inner layer
368 also appears to facilitate the continued growth of pits, partially aided by enabling easier access

of the electrolyte to the steel surface in comparison to the compact crystalline $FeCO_3$ layer on the X65 steel surface. In contrast, the inner layer on X65 steel comprised solely of $FeCO_3$ and was able to reduce the general corrosion rate the most effectively compare to the Cr steels, whilst also preventing the propagation of pits beyond 96 h of exposure.

Another key observation is the $FeCO_3$ crystal size on the surfaces of the different steels. Increasing Cr content within the steel resulted in larger (and fewer) $FeCO_3$ crystals forming within the outer layer (shown in Figure 4). The porosity of the outer layer visibly increases with Cr content in the steel, with an increase in crystal size and reduction in compactness. This correlates with the increase in general corrosion rate with Cr content, suggesting that the outer film may be responsible for providing some protection to the steel surface (although the majority of protection appears to be afforded by the inner layer in the case of the low Cr steels).

The larger, more discrete crystals at higher Cr content indicate a reduction in nucleation and enhanced growth with increasing Cr content in the steel. This can be explained by reviewing how the nucleation and growth characteristics change with the saturation ratio (SR) of $FeCO_3$, which is essentially a measure of the extent to which the solubility limit is exceeded[28]:

$$SR = \frac{[Fe^{2+}][CO_3^{2-}]}{K_{SP}} \quad (6)$$

where SR is the saturation ratio of $FeCO_3$, $[Fe^{2+}]$ and $[CO_3^{2-}]$ are the concentrations of iron and carbonate ions in mol/L and $K_{sp}$ is the solubility product for $FeCO_3$ in $mol^2/L^2$.

The nucleation rate of $FeCO_3$ varies exponentially with SR, while growth varies linearly. Consequently, high SR values result in high nucleation and less growth, while lower SR results in less nucleation and greater growth [24]. This suggests that the SR of the solution at the location of $FeCO_3$ precipitation on the outer surface reduces as the Cr content in the steel increases. The growth of the outer film is also delayed as the Cr content in the steel increases. Both these observations correlate with the slower release of $Fe^{2+}$ ions from the steel surface with increasing Cr content during the earlier stages of corrosion. As the $Fe^{2+}$ flux from the surface reduces with increasing steel Cr content (due to the suppression of corrosion rate from the $Cr(OH)_3$ film), the solution will take longer to become saturated with respect to $FeCO_3$ and will not reach as high values of SR, resulting in the development of larger, more discrete crystals within the outer layer.

## *6 Conclusions*

In this work, the corrosion behaviour of X65, 1Cr, 3Cr and 5Cr steel exposed to $CO_2$-saturated 1 wt.% NaCl brine at 60°C and 100 bar for various immersions times was studied. The findings from this work are as follows:

1. In the early stages of corrosion, in the absence of significant corrosion product formation, the general corrosion rate of X65 exhibited the highest corrosion rate (16.7 mm/year). Corrosion resistance of the four materials increased with increasing Cr content (corrosion resistance: X65<1Cr<3Cr<5Cr), the presence of low Cr content (1-5%) produced a chromium hydroxide ($Cr(OH)_3$) film in the first 6 h of exposure to the test solution. Increasing Cr content within the steel proved beneficial toward mitigating material dissolution in the absence of formation of protective corrosion products, suppressing corrosion rate by a factor of 2.5 for 5Cr steel over the first 6 h.
2. Longer durations of exposure for all materials resulted in the formation of protective corrosion products consisting of a duplex structure (an inner amorphous/nano-crystalline layer and an outer crystalline layer). The outer layer on all samples comprised of solely $FeCO_3$. The inner layer for X65 consisted of $FeCO_3$ only, while for Cr steel, contained significant levels of Cr enrichment as a result of $Cr(OH)_3$ presence, as well as trace amounts of $FeCO_3$.
3. After 192 h of exposure, the thickness of the corrosion products were very similar (60 µm), but offered different levels of protection against general and localised corrosion. The Cr enrichment of the inner film appeared to facilitate continued pit propagation, with a reduction in general corrosion protection being observed with increasing Cr content in the steel and the film.
4. The corrosion product layer formed on X65 steel after 192 h was able to significantly suppress general corrosion (corrosion resistance: X65>1Cr>3C>5Cr). The extent of localised corrosion decreased significantly for X65 as it became covered by dense and compact $FeCO_3$ compared to the Cr-containing steels, and increasing Cr content failed to improve localised corrosion resistance.
5. The presence of Cr in the steels influenced the nucleation and growth characteristics of $FeCO_3$ crystals on the outer layer which was predominantly due to the rate of release of

$Fe^{2+}$ ions into the solution in the earlier stages of corrosion, resulting in different saturation ratios at the location of $FeCO_3$ precipitation.

6. The work also highlighted that individual mass loss tests at a specific time intervals can result in the misinterpretation of material corrosion resistance ranking when protective corrosion products develop on steel surfaces. Multiple experiments over the film formation period are required to fully characterise material behaviour in the presence of such films to produce reliable conclusions regarding the protection afforded by corrosion products. The results indicate that the low Cr steels are no more suitable for this situation compared to X65 carbon steel under the tests conditions considered here.

## *5. References*


1. Ikeda, A., M. Ueda, and S. Mukai, $CO_2$ Behavior of Carbon and Chromium Steels.(Retroactive Coverage). Advances in $CO_2$ Corrosion., 1984. 1: p. 39-51.
2. J. Crolet, N. Thevenot, and S. Nesic, Role of Conductive Corrosion Products in the Protectiveness of Corrosion Layers. Corrosion, 1998. 54(3): p. 194-203.
3. S. Nesic and L. Lunde, Carbon dioxide corrosion of carbon steel in two-phase flow. Corrosion, 1994. 50(9): p. 717-727.
4. E.P. DeGarmo, J.T. Black, R.A. Kohser, and B.E. Klamecki, Materials and process in manufacturing. 1997: Prentice Hall.
5. L.N. Xu, S.Q. Guo, W. Chang, T.H. Chen, L.H. Hu, and M.X. Lu, Corrosion of Cr bearing low alloy pipeline steel in $CO_2$ environment at static and flowing conditions. Applied Surface Science, 2013. 270: p. 395-404.
6. L. Xu, B. Wang, J. Zhu, W. Li, and Z. Zheng, Effect of Cr content on the corrosion performance of low-Cr alloy steel in a $CO_2$ environment. Applied Surface Science, 2016. 379: p. 39-46.
7. J. Sun, C. Sun, and Y. Wang, Effect of Cr Content on the Electrochemical Behavior of Low-chromium X65 Steel in $CO_2$ Environment. Int. J. Electrochem. Sci, 2016. 11: p. 8599-8611.
8. C. Chen, M. Lu, D. Sun, Z. Zhang, and W. Chang, Effect of chromium on the pitting resistance of oil tube steel in a carbon dioxide corrosion system. Corrosion, 2005. 61(6): p. 594-601.
9. M.B. Kermani and A. Morshed, Carbon Dioxide Corrosion in Oil and Gas Production - A Compendium. Corrosion, 2003. 59(8): p. 659-683.
10. S.Q. Guo, L.N. Xu, L. Zhang, W. Chang, and M.X. Lu, Corrosion of Alloy Steels Containing 2% Chromium in $CO_2$ Environments. Corrosion Science, 2012. 63: p. 246-258.

11. R. Barker, Y. Hua, and A. Neville, Internal corrosion of carbon steel pipelines for dense-phase $CO_2$ transport in carbon capture and storage (CCS)–a review. International Materials Reviews, 2017. 62(1): p. 1-31.
12. J.B. Sun, W. Liu, W. Chang, Z.H. Zhang, Z.T. Li, T. Yu, and M.X. Lu, Characteristics and formation mechanism of corrosion scales on low-chromium X65 steels in $CO_2$ environment. Acta Metall Sin, 2009. 45(1): p. 84.
13. J. Sun, C. Sun, X. Lin, X. Cheng, and H. Liu, Effect of chromium on corrosion behavior of P110 steels in $CO_2$-$H_2S$ environment with high pressure and high temperature. Materials, 2016. 9(3): p. 200.
14. K. Nose, H. Asahi, P. I. Nice, and J. W. Martin. Corrosion properties of 3% Cr steels in oil and gas environments. in CORROSION 2001. 2001. NACE International.
15. S. Hassani, T.N. Vu, N.R. Rosli, S.N. Esmaeely, Y.-S. Choi, D. Young, and S. Nesic, Wellbore integrity and corrosion of low alloy and stainless steels in high pressure $CO_2$ geologic storage environments: An experimental study. International Journal of Greenhouse Gas Control, 2014. 23: p. 30-43.
16. T. Muraki, T. Hara, and H. Asahi. Effects of chromium content up to 5% and dissolved oxygen on $CO_2$ corrosion. in CORROSION 2002. 2002. NACE International.
17. S. Zhang, L. Hou, Y. Wei, H. Du, H. Wei, B. Liu, and X. Chen, Dual functions of chloride ions on corrosion behavior of mild steel in $CO_2$ saturated aqueous solutions. Materials and Corrosion.
18. S. Zhang, L. Hou, H. Wei, Y. Wei, and B. Liu, Failure analysis of an oil pipe wall perforated by pitting corrosion. Materials and Corrosion, 2018. 69(8): p. 1123-1130.
19. L. Hou, M. Raveggi, X.-B. Chen, W. Xu, K.J. Laws, Y. Wei, M. Ferry, and N. Birbilis. Investigating the passivity and dissolution of a corrosion resistant Mg-33at.% Li alloy in aqueous chloride using online ICP-MS. Journal of The Electrochemical Society 2016 [cited 163 6]; C324-C329].
20. B. Kermani, J.C. Gonzales, G.L. Turconi, T.E. Perez, and C. Morales. In-field corrosion performance of 3% Cr steels in sweet and sour downhole production and water injection. in CORROSION 2004. 2004. NACE International.
21. A. Dugstad, H. Hemmer, and M. Seiersten, Effect of steel microstructure on corrosion rate and protective iron carbonate film formation. Corrosion, 2001. 57(4): p. 369-378.

22. B. Kermani, M. Dougan, J.C. Gonzalez, C. Linne, and R. Cochrane. Development of low carbon Cr-Mo steels with exceptional corrosion resistance for oilfield applications. in CORROSION 2001. 2001. NACE International.
23. A. Kumar, S.K. Desai, J.L. Pacheco, W. Sun, W. Huang, and M. Asmann. Corrosion Performance of L80-1Cr and L80-3Cr Oil Country Tubular Goods (OCTG) in High $CO_2$ at Elevated Temperature. in CORROSION 2013. 2013. NACE International.
24. R. Elgaddafi, A. Naidu, R. Ahmed, S. Shah, S. Hassani, S.O. Osisanya, and A. Saasen, Modeling and experimental study of $CO_2$ corrosion on carbon steel at elevated pressure and temperature. Journal of Natural Gas Science and Engineering, 2015. 27: p. 1620-1629.
25. Y. Hua, A. Shamsa, R. Barker, and A. Neville, Protectiveness, morphology and composition of corrosion products formed on carbon steel in the presence of $Cl^-$, $Ca^{2+}$ and $Mg^{2+}$ in high pressure $CO_2$ environments. Applied Surface Science, 2018. 455: p. 667-682.
26. M. Ueda and H. Takabe. The formation behavior of corrosion protective films of low Cr bearing steels in $CO_2$ environments. in CORROSION 2001. 2001. NACE International.
27. Y. Xiang, H. Huang, Z. Long, C. Li, and W. Yan, Role of residual 2-amino-2-methyl-1-propanol and piperazine in the corrosion of X80 steel within an impure supercritical $CO_2$ environment as relevant to CCUS. International Journal of Greenhouse Gas Control, 2019. 82: p. 127-137.
28. A. Pfennig and R. Bäßler, Effect of $CO_2$ on the stability of steels with 1% and 13% Cr in saline water. Corrosion Science, 2009. 51(4): p. 931-940.
29. ASTM, E3-01. 2002: Standard Practice for Preparation of Metallographic Specimens. Annual Book of ASTM Standards, ASTM.
30. ASTM, E 407–99, Standard Guide for Microetching Metals and Alloys. American Society for Testing Materials.
31. Y. Hua, R. Barker, and A. Neville, Comparison of corrosion behaviour for X-65 carbon steel in supercritical $CO_2$-saturated water and water-saturated/unsaturated supercritical $CO_2$ The Journal of Supercritical Fluids, 2015. 97: p. 224-237.
32. Y. Hua, R. Barker, and A. Neville, Effect of temperautre on the critical water content for general and localised corrosion of X65 carbon steel in the transport of supercritical $CO_2$. The International Journal of Greenhouse Gas Control, 2014. 31: p. 48-60.
33. Y. Hua, R. Barker, C. T, M. Ward, and A. Neville, Relating Iron Carbonate Morphology to Corrosion Characteristics for Water-Saturated Supercritical $CO_2$ Systems. The Journal of Supercritical Fluids, 2014. vol. 98: p. 183-193.

34. MultiScale 7.1 is a commercial software package from Expro Group International Ltd, for more information see: http://multiscale.no/.
35. ASTM, Standard G1-03, Standard practice for preparing, cleaning, and evaluating corrosion test specimens. ASTM International: West Conshohocken, PA, 2003.
36. ASTM, Standard G46-94, Standard guide for examination and evaluation of pitting corrosion. ASTM International: West Conshohocken, PA, 2003.
37. M.H. Nazari, S. Allahkaram, and M. Kermani, The effects of temperature and pH on the characteristics of corrosion product in $CO_2$ corrosion of grade X70 steel. Materials & Design, 2010. 31(7): p. 3559-3563.
38. A. Dugstad, Mechanism of Protective Film Formation During $CO_2$ Corrosion of Carbon Steel, in CORROSION 981998, NACE International: Sand Diego, CA:NACE.
39. W. Sun and S. Nesic, Basics revisited: kinetics of iron carbonate scale precipitation in $CO_2$ corrosion. Corrosion/2006, paper, 2006(06365).
40. A. Dugstad, The importance of $FeCO_3$ supersaturation on the $CO_2$ corrosion of mild steels. CORROSION/92, paper, 1992(14).

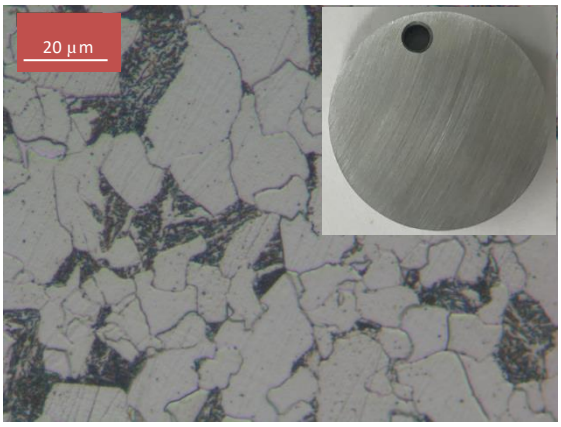


**(a)**

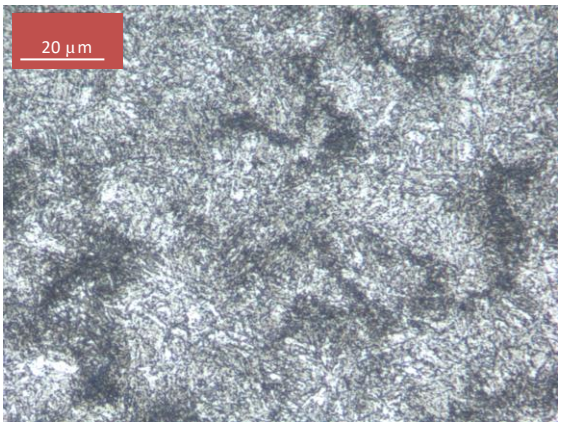


**(b)**

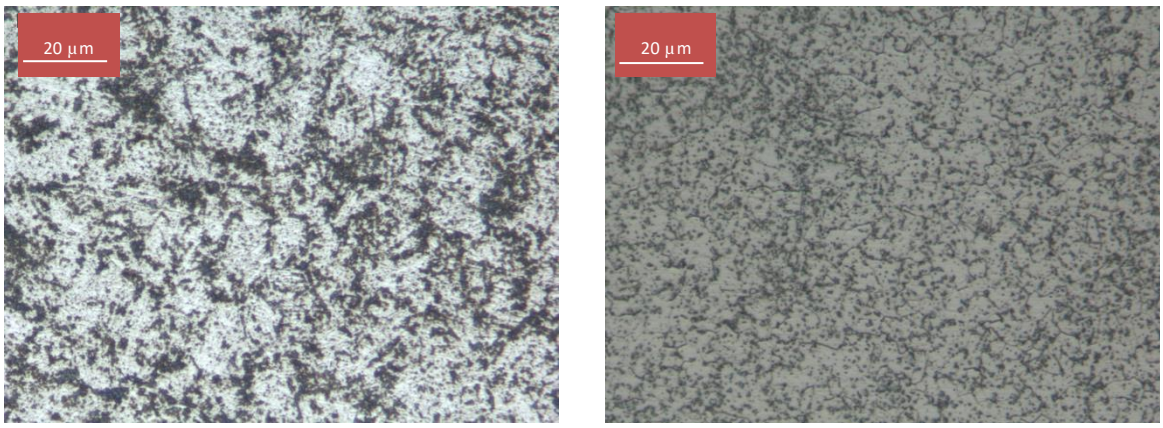


(c) (d)

537 **Figure 1: Optical microscope images of microstructures for (a) X65, (b) 1Cr, (c) 3Cr and (d)**
538 **5Cr. Note: A typical sample coupon is shown in the insert in (a).**

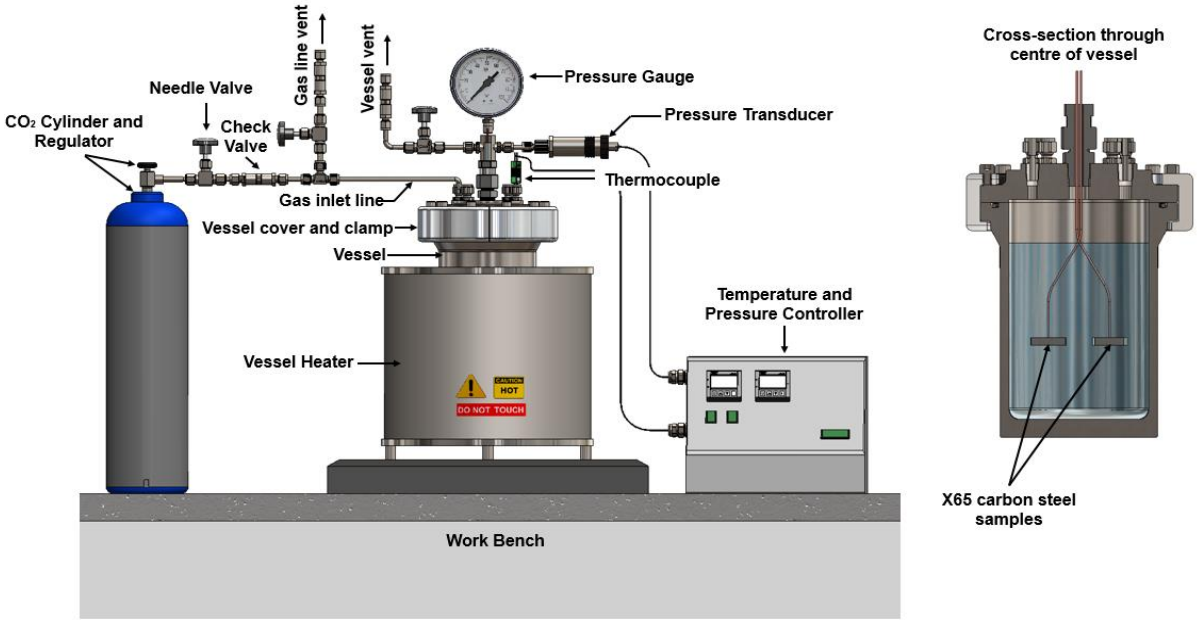


539

540 **Figure 2: Schematic of autoclave setup**

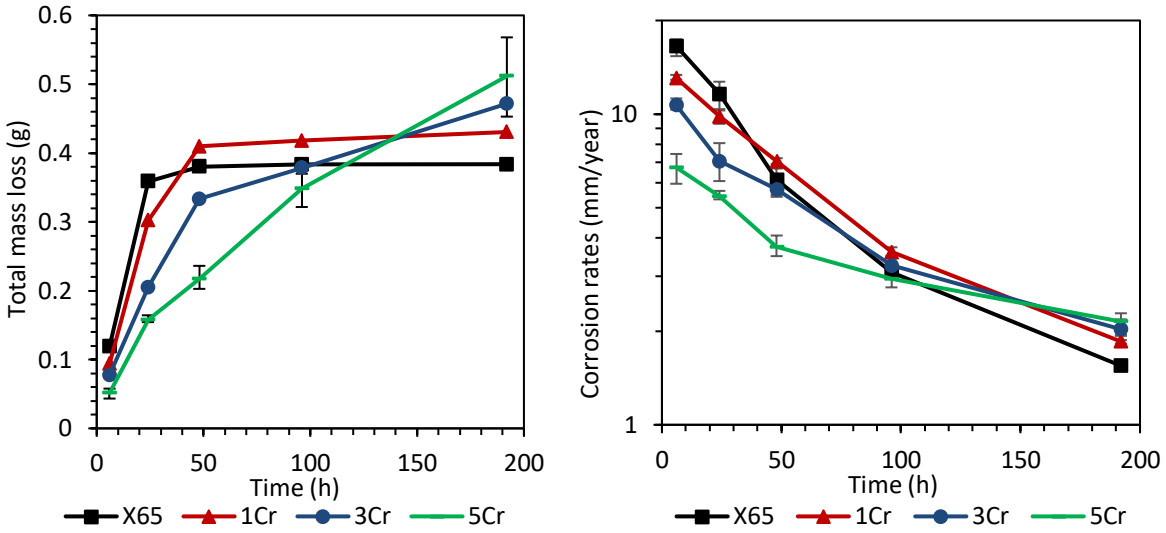


(a) (b)

**Figure 3: Plots depicting (a) total mass loss and (b) general corrosion rates for X65, 1Cr, 3Cr and 5Cr steel exposed to a $CO_2$-saturated 1 wt.% NaCl solution at various immersion times at 60°C and 100 bar**

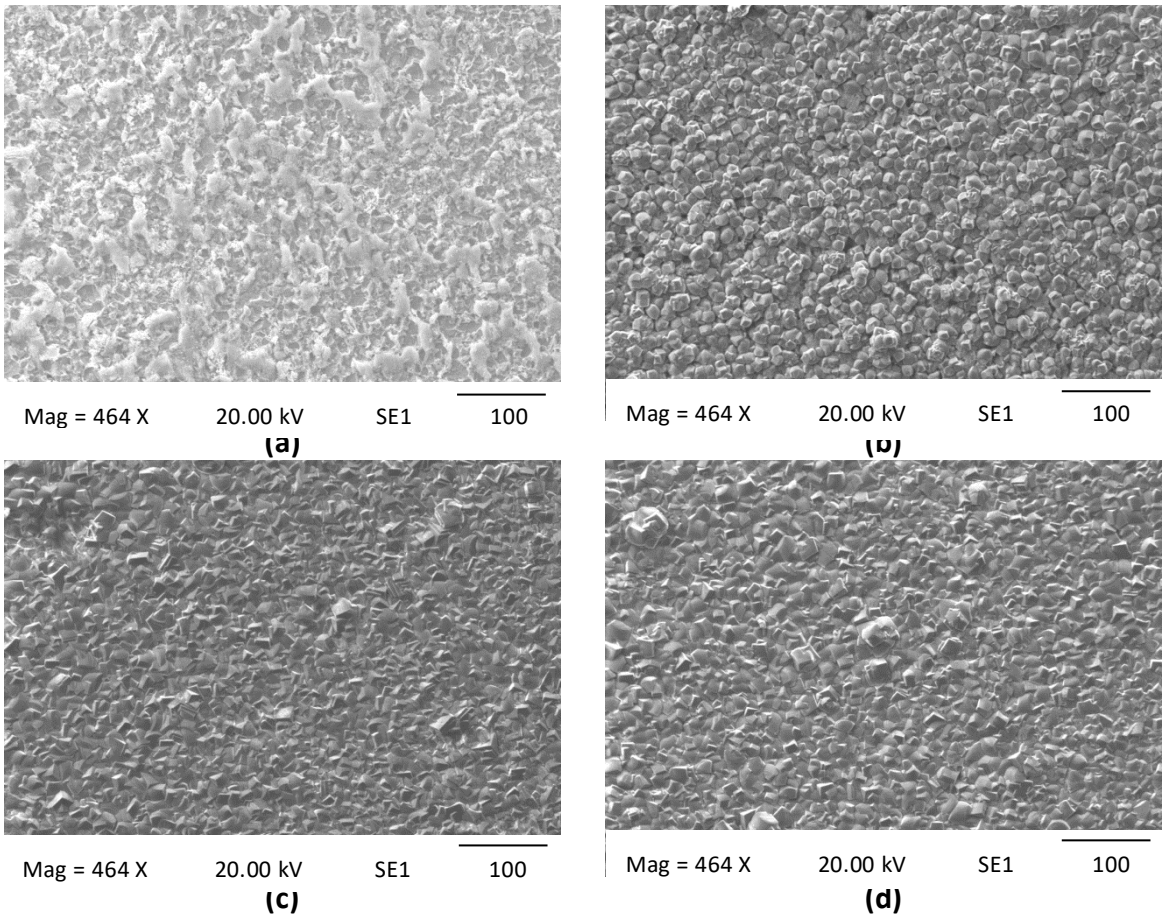

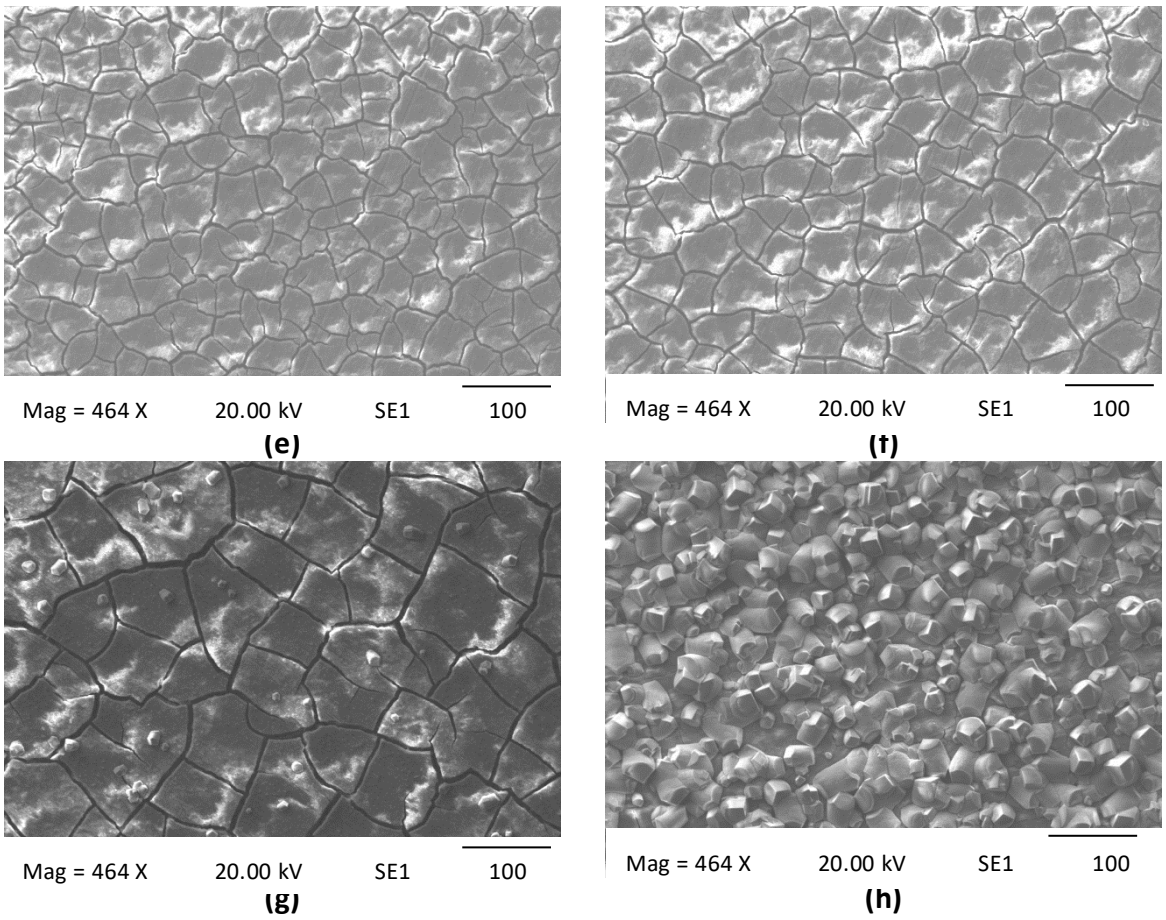


**Figure 4: SEM images of surface morphology of corrosion products formed on X65 exposed to a $CO_2$-saurated 1 wt.% NaCl solution at 60°C and 100 bar for various immersion periods of (a) 6 h, (b) 24 h, (c) 96 h and (d) 192 h. The corrosion products for 5Cr exposed to a $CO_2$-saurated 1 wt.% NaCl solution at 60°C and 100 bar for immersion periods of (e) 6 h, (f) 24 h, (g) 96 h and (h) 192 h. The corresponding cross-sections are provided in Figures 5 and 6.**

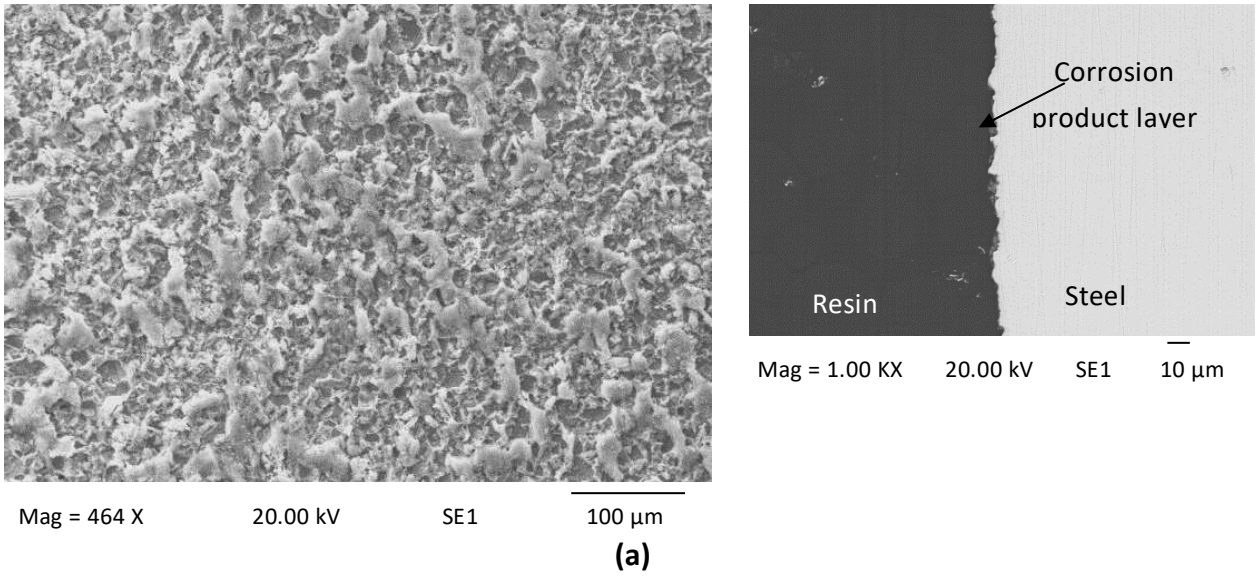

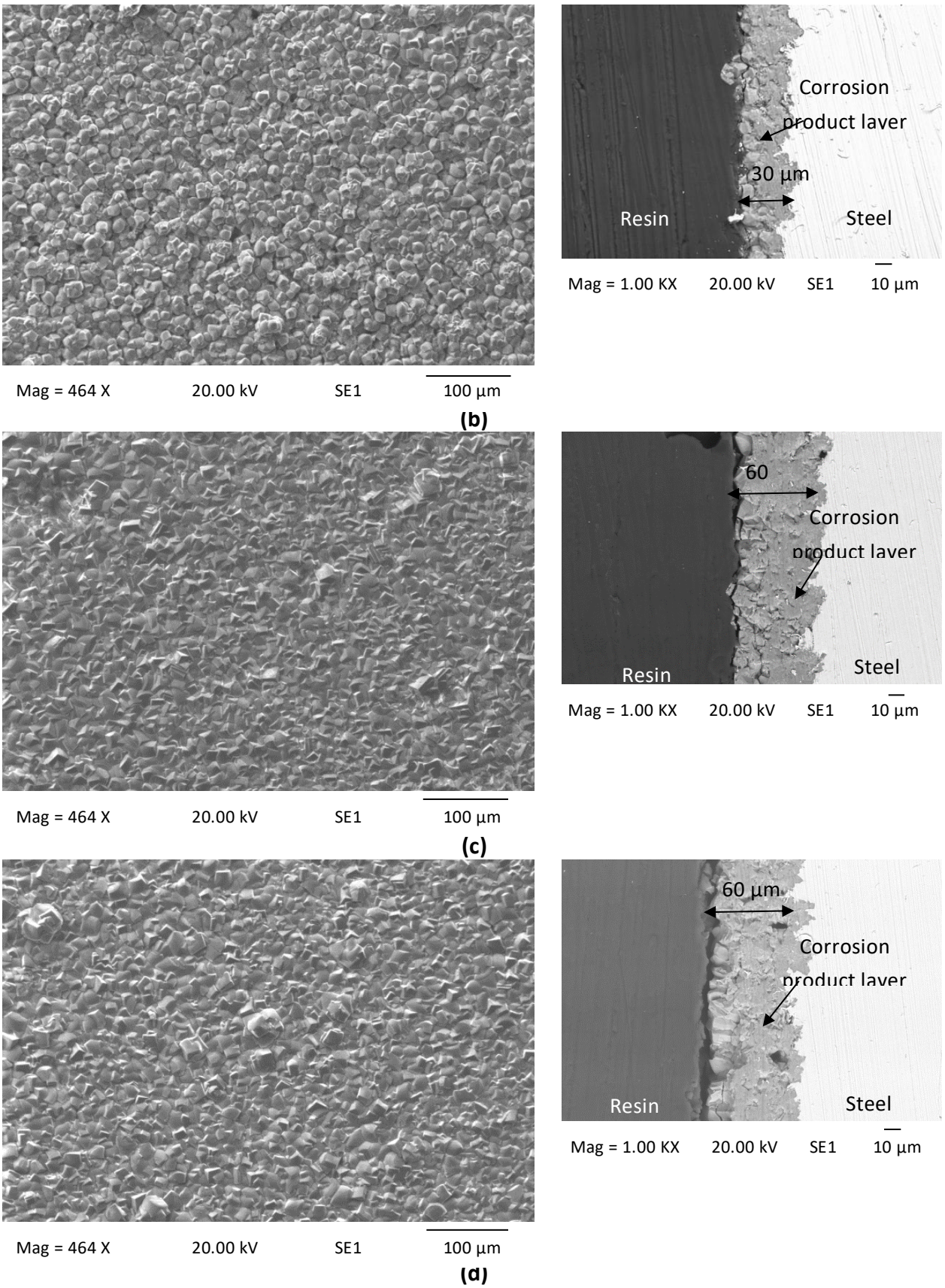


**Figure 5: SEM images of surface morphology and corresponding cross sections of corrosion products formed on X65 carbon steel exposed to a $CO_2$-saturated 1 wt.% NaCl solution at 60°C and 100 bar for various immersion periods of (a) 6 h, (b) 24 h, (c) 96 h and (d) 192 h.**

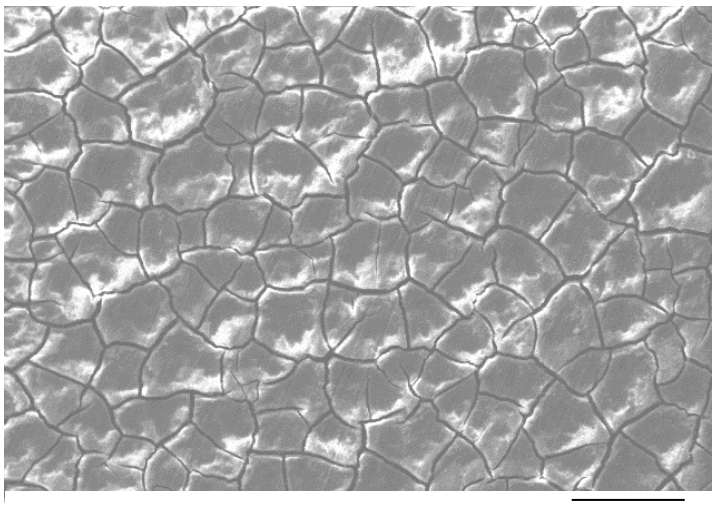
Mag = 464 X
20.00 kV
SE1
100 µm

(a)

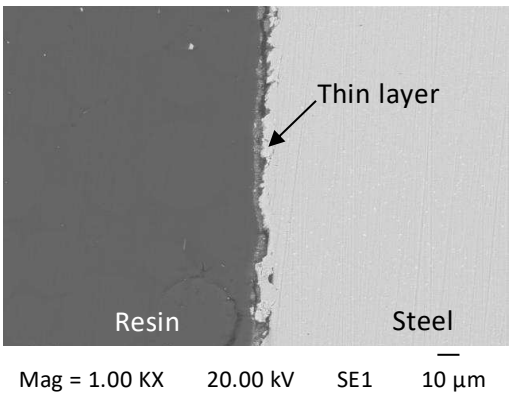
Thin layer
Resin
Steel
Mag = 1.00 KX
20.00 kV
SE1
10 µm

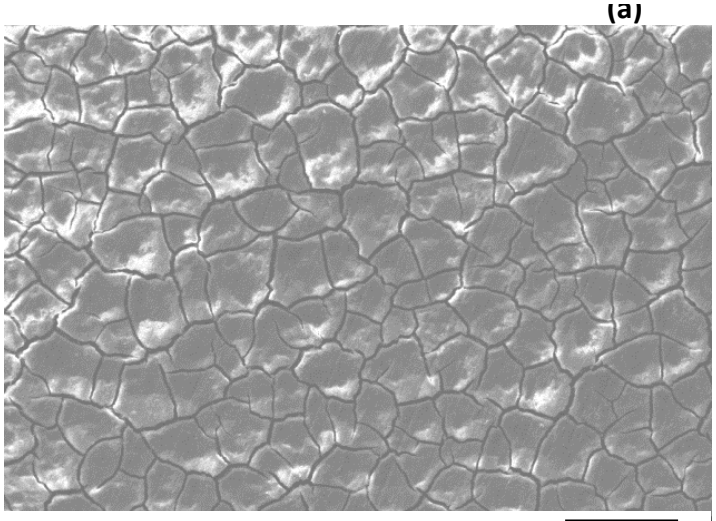
Mag = 464 X
20.00 kV
SE1
100 µm

(b)

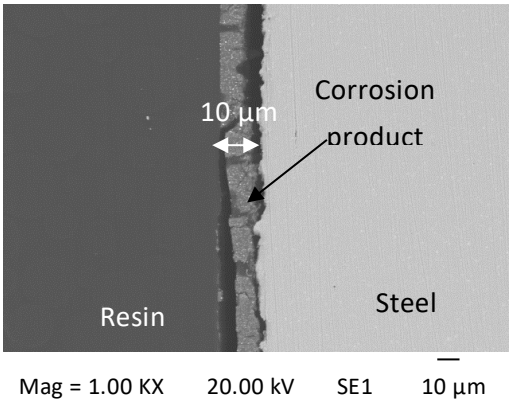
10 µm
Corrosion
product
Resin
Steel
Mag = 1.00 KX
20.00 kV
SE1
10 µm

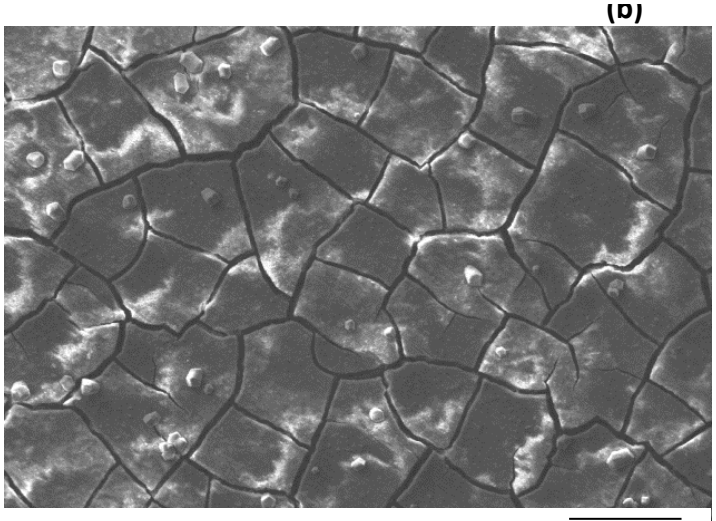
Mag = 464 X
20.00 kV
SE1
100 µm

(c)

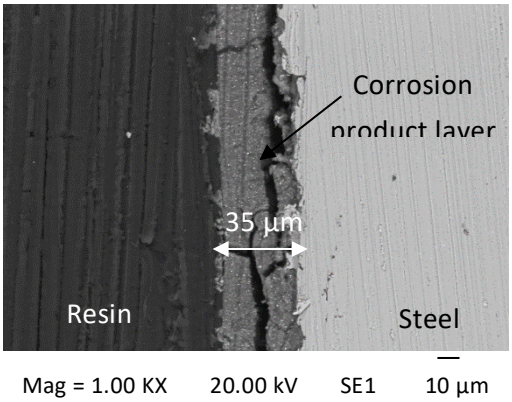
Corrosion
product layer
35 µm
Resin
Steel
Mag = 1.00 KX
20.00 kV
SE1
10 µm

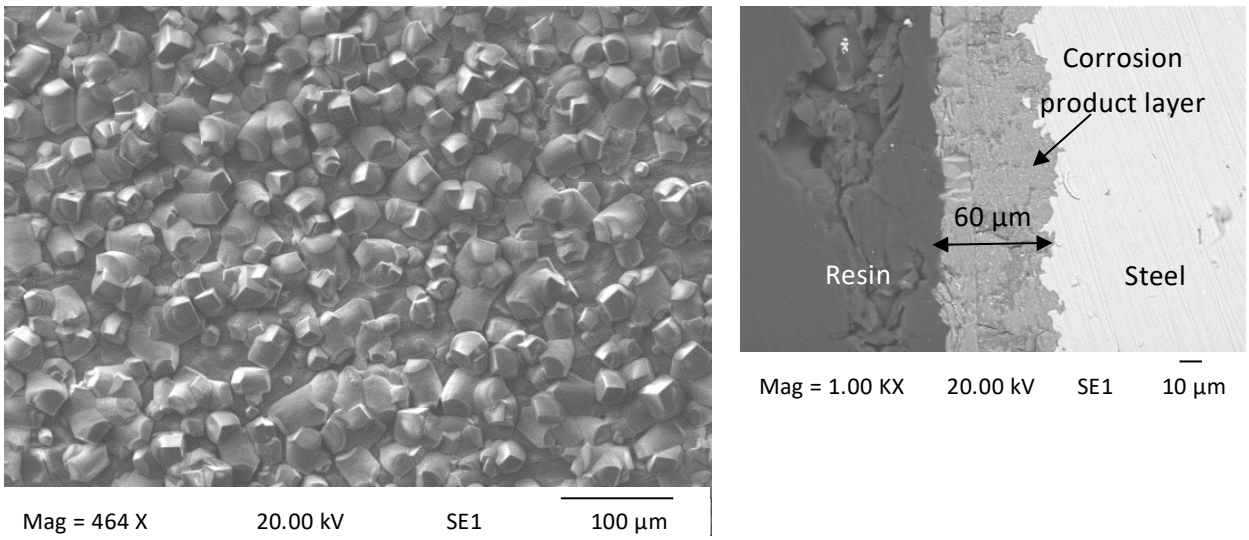


**Figure 6: SEM images of surface morphology and corresponding cross sections of corrosion products formed on 5Cr steel exposed to a $CO_2$-saturated 1 wt.% NaCl solution at 60°C and 100 bar for various immersion periods of (a) 6 h, (b) 24 h, (c) 96 h and (d) 192 h.**

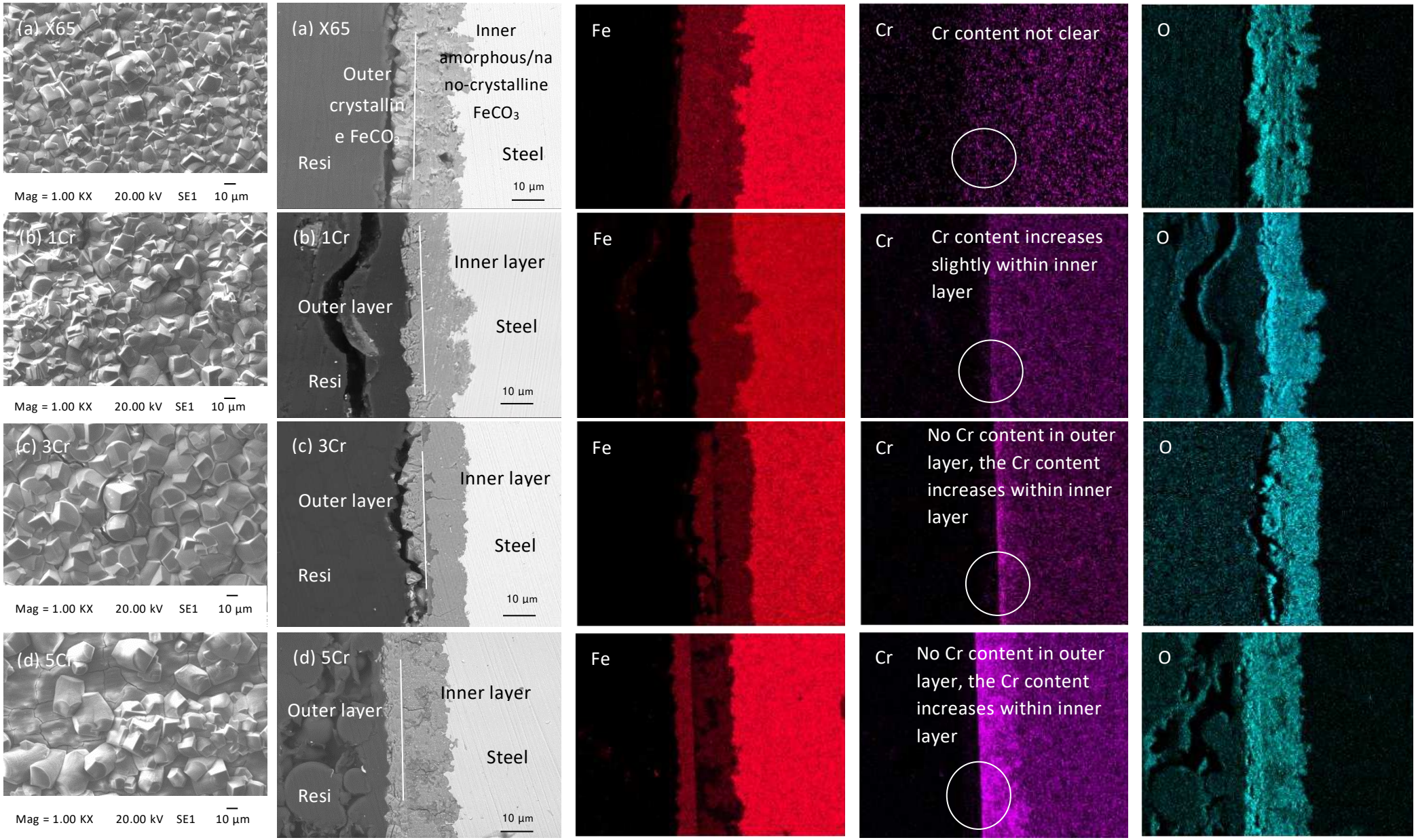


**Figure 7: SEM cross-section images and EDX maps of (a) X65, (b) 1Cr, (c) 3Cr and (d) 5Cr samples exposed to $CO_2$-saturated solution at 100 bar and 60°C for 192 h.**

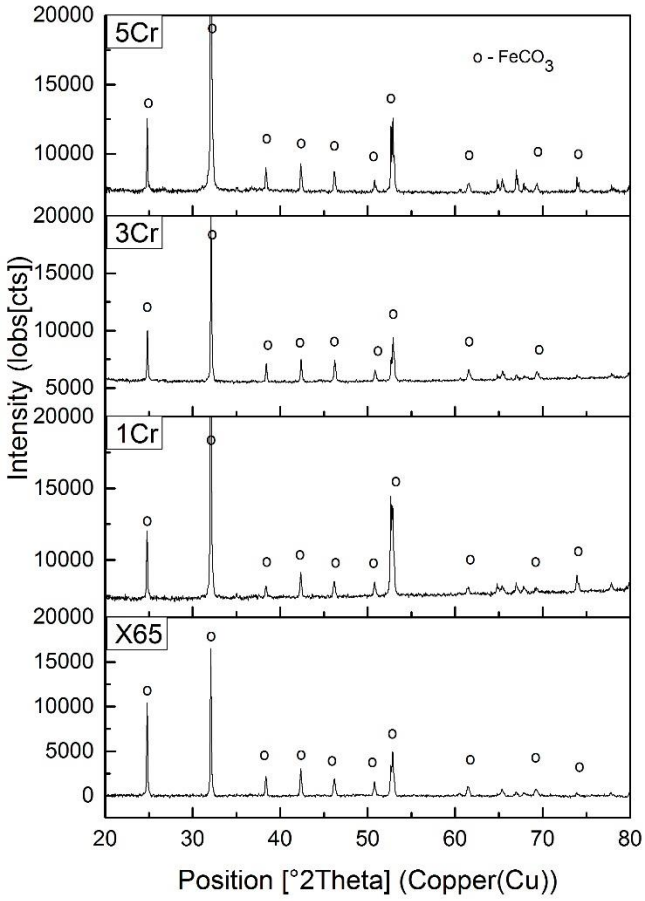


**Figure 8: XRD patterns of X65, 1Cr, 3Cr and 5Cr samples exposed to a $CO_2$-saturated 1 wt.% NaCl solution at 100 bar and 60°C for 192 h.**

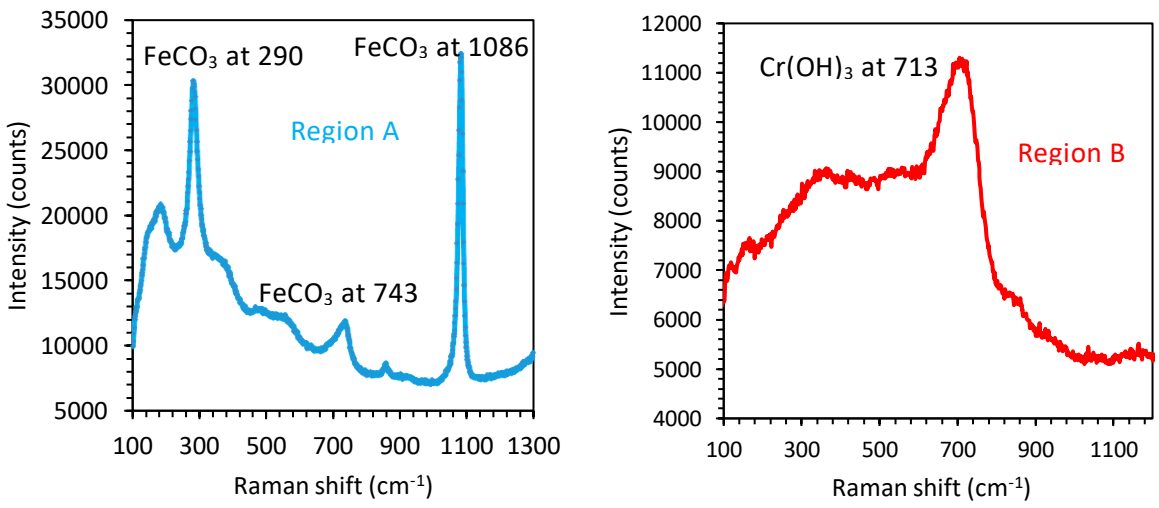

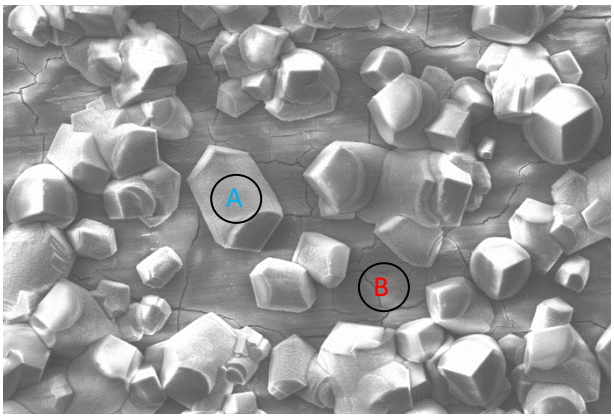


**Figure 9: Raman spectroscopy of the corrosion products at particular positions from 5Cr steel exposed to a $CO_2$-saturated 1 wt.% NaCl solution at 60°C and 100 bar for 192 h**

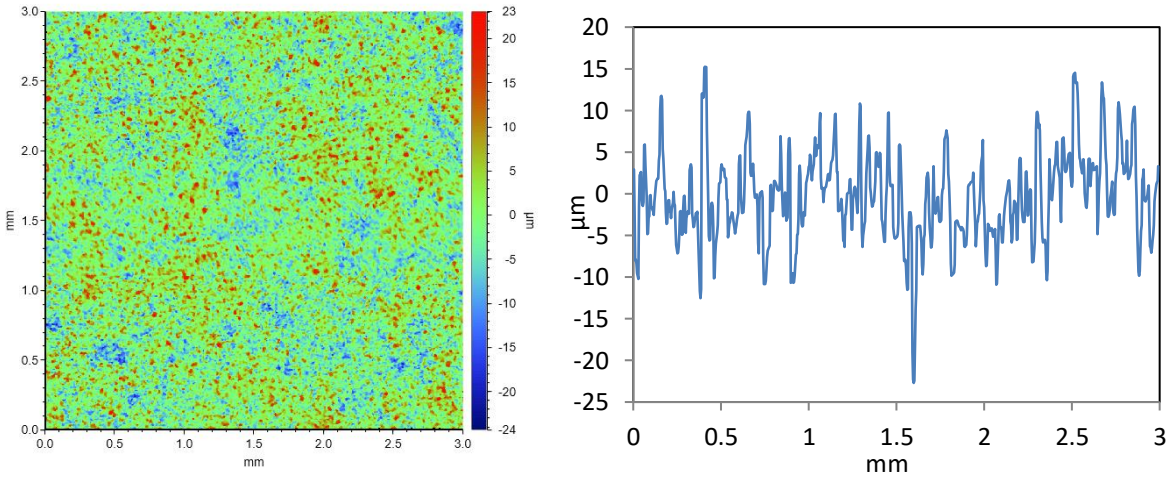


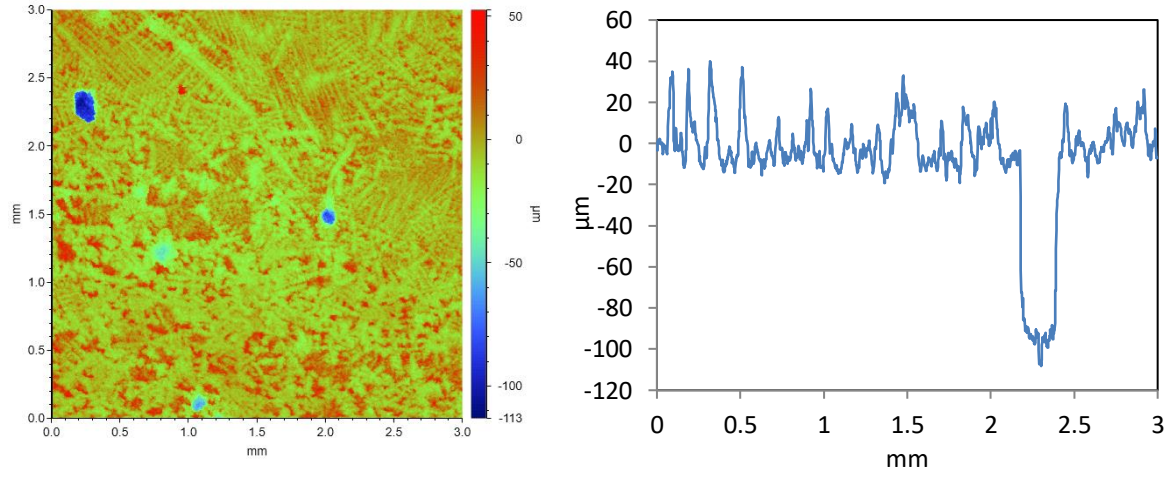

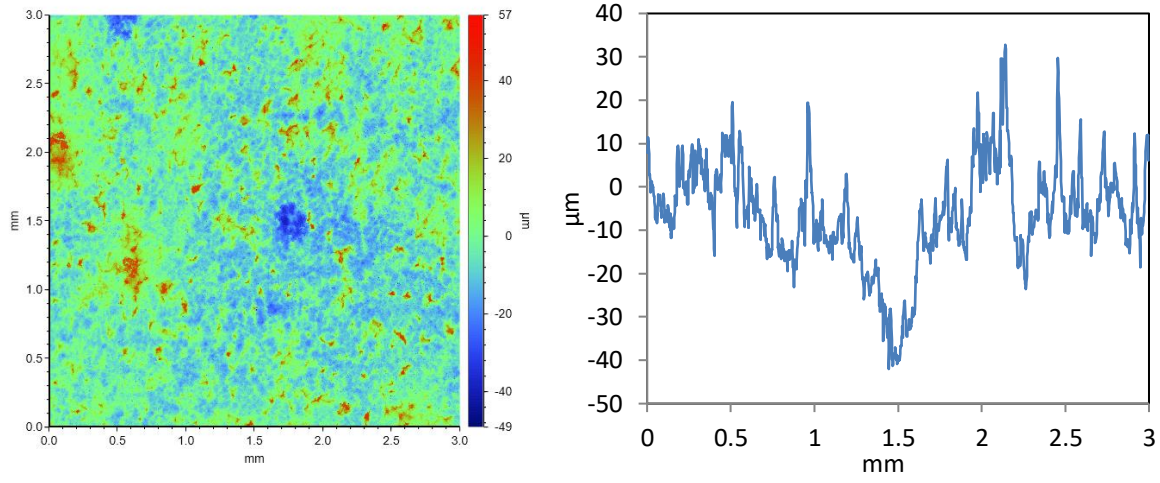


583

584

585

586

587 **Figure 10: Example of profilometry images for (a) X65, (b) 1Cr, (c) 3Cr and (d) 5Cr steel**
588 **surfaces after removal of corrosion products after exposure to a $CO_2$-saturated 1 wt.% NaCl**
589 **solution at 100 bar and 60°C for 192 h.**

590

591

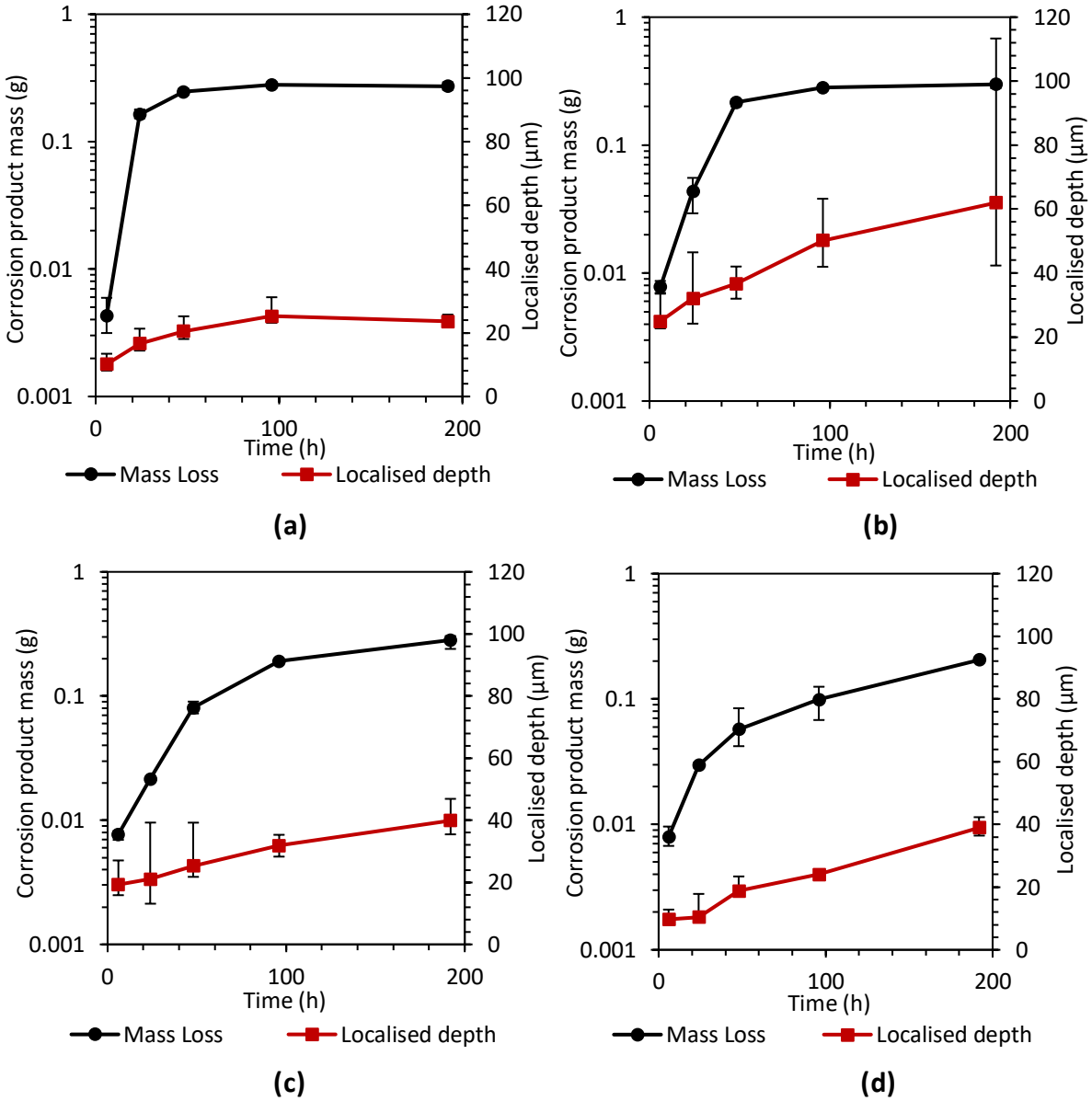


**Figure 11: Mass of corrosion products formed on sample surface and measured pit depth for (a) X65, (b) 1Cr, (c) 3Cr and (d) 5Cr exposed to a $CO_2$-saturated 1 wt.% NaCl solution at 60 °C and 100 bar at various immersion time.**

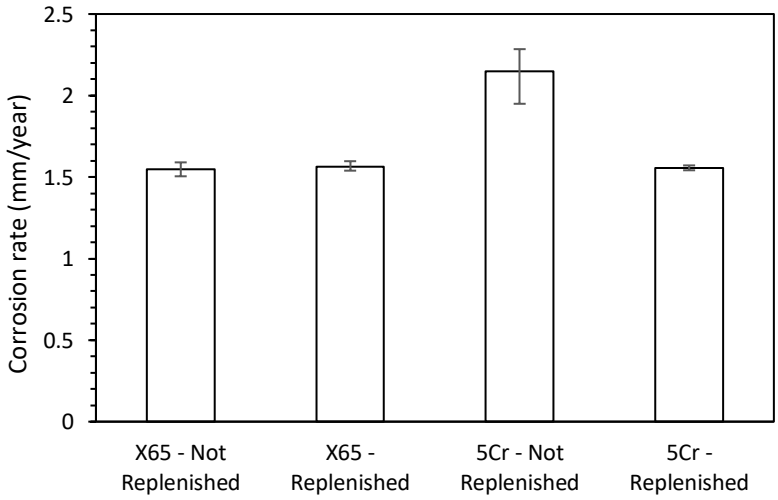

**Figure 12: Corrosion rates for X65 and 5Cr after 192 h exposure to a $CO_2$-saturated 1 wt.% NaCl solution at 60 °C and 100 bar. The graphs illustrate the effect of replenishing the test solution after 48 h.**

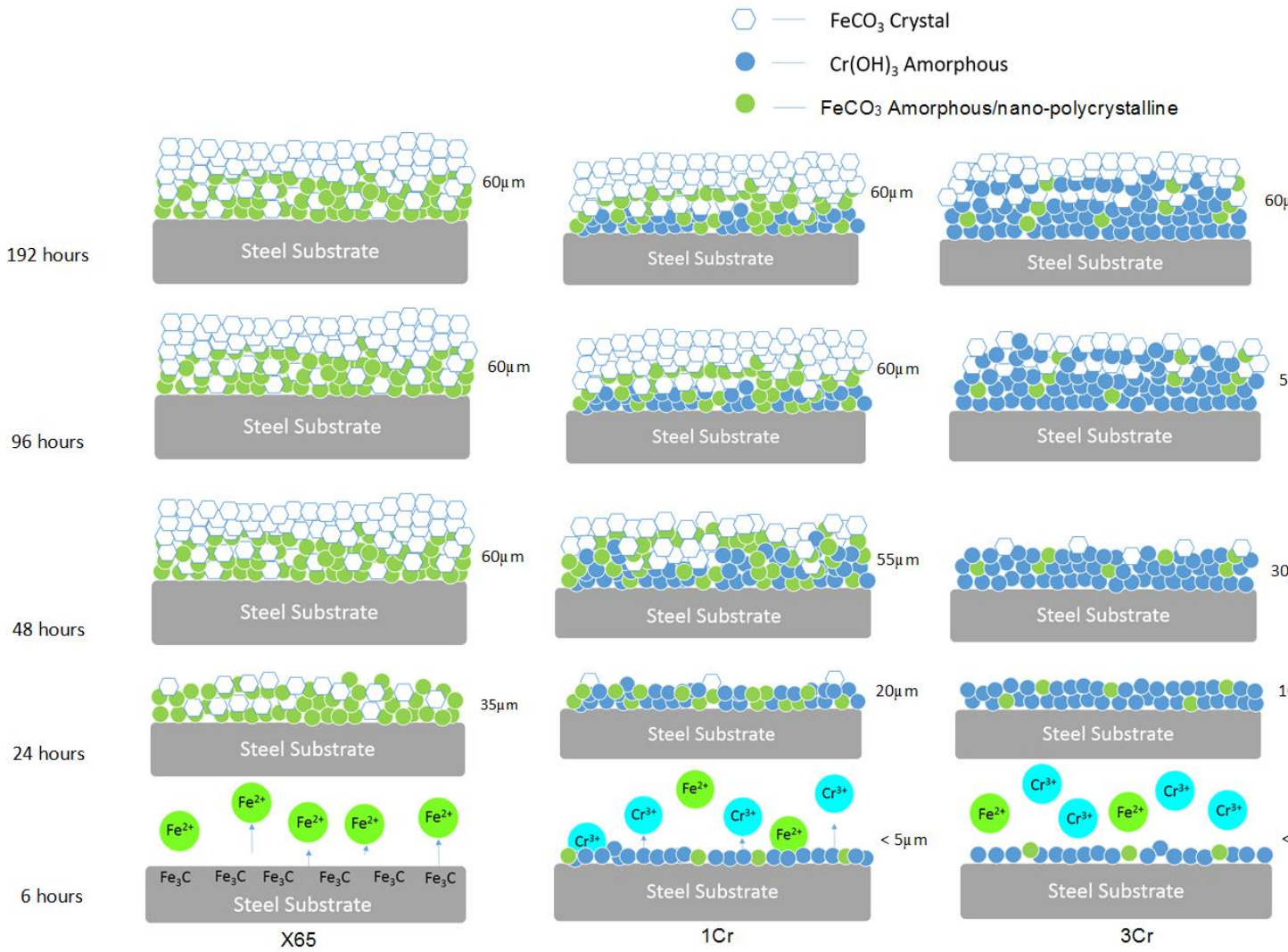


Figure 13: Schematic model for the corrosion product evolution of inner and outer layer on X65, 1Cr, 3Cr and 5Cr steels.

608

609 **Table 1: Elemental compositions of X65, 1Cr, 3Cr and 5Cr steels (wt.%)**

| | X65 | 1Cr | 3Cr | 5Cr |
|---|---|---|---|---|
| C | 0.12 | 0.35 | 0.24 | 0.35 |
| Si | 0.18 | 0.35 | 0.21 | 0.85 |
| Mn | 1.27 | 0.75 | 0.53 | 0.4 |
| P | 0.008 | 0.035 | 0.005 | 0.012 |
| S | 0.002 | 0.05 | 0.0015 | 0.002 |
| Cr | 0.11 | 1.12 | 3.10 | 5.00 |
| Fe | Balance | | | |

610

611

612